Use of a birefringent filter for tuning a synchronously pumped optical parametric oscillator

Martin V. O'Connor, Malcolm A. Watson, David P. Shepherd, and David C. Hanna

Optoelectronics Research Centre, University of Southampton, Southampton SO17 1BJ, UK

Fax: +44 (0)23 80593142

Email: moc@orc.soton.ac.uk

ABSTRACT. Design considerations are presented for birefringent filters suitable for use as tuning elements in synchronously pumped optical parametric oscillators. A particular design aspect that is important, since typical gains are rather high, is the adequate suppression of subsidiary transmission maxima, in order to maximize the tuning range. Results are presented on the performance of a picosecond synchronously pumped optical parametric oscillator based on periodically poled lithium niobate with an appropriately designed 4-plate birefringent filter.

PACS: 42.65.Yj, 42.72.Ai

1. Introduction

In many optical parametric oscillator (OPO) systems it has been common practice to rely solely on the parametric gain profile to provide frequency selection of the oscillating waves. Tuning can then be achieved by shifting the peak of the gain profile (e.g. by temperature-tuning or angle-tuning of the nonlinear crystal or by tuning the pump frequency), relying on the fact that the oscillation frequency corresponds to the gain peak. However, there are often situations where additional frequency control can be beneficial and various frequency selection elements have been used for this (e.g. etalons, gratings). One obvious benefit from including a tuning element/filter can be the more agile tuning compared with the slow process of temperature-tuning. Recent papers have reported the use of a diffraction grating as a frequency selective feedback 'mirror' in a synchronously pumped OPO (SPOPO) based on periodically poled lithium niobate (PPLN) [1,2]. There it was shown that, besides the benefit of greater agility than with temperature-tuning, the filter-action of the grating was helpful in reducing sensitivity to frequency-pulling effects caused by cavity-length detuning, these effects being a general feature of SPOPOs [2]. Further benefits observed were the ability to operate very close to degeneracy [1], while still preserving singly-resonant operation, and the ability to tune through atmospheric absorption arising within the air path in the OPO resonator, without suffering frequency jumps of the signal away from the absorption [2]. A further benefit is the suppression of additional unwanted oscillation frequencies, which can accompany the signal in high-gain SPOPOs based on quasi-phase-matched materials such as PPLN. The precise origin of these additional frequency components has not been definitely identified (see Ref. 3 for examples of the resulting complex output spectra), but nonlinear processes such as stimulated Raman scattering and higher-order-mixing processes in the PPLN are possible contributors. These can be very

effectively eliminated by intracavity filtering and such a use of a grating was an important aspect of a recently reported Cadmium Selenide SPOPO pumped by a PPLN SPOPO [4].

Thus, quite apart from the tuning capability, there are compelling reasons for using an intracavity tuning element, in terms of the spectrally cleaner and more stable performance of the SPOPO. While the use of a grating has been demonstrated to be a practical approach, it has some drawbacks and for this reason we have investigated the alternative of using a birefringent filter (BF). In fact, the use of a BF in a SPOPO has been reported previously for a low-gain device operating with rather long pulses (20-30 ps) [5], although no detail was given of the filter design and characteristics. Here, we present a detailed discussion of the BF design strategy and of the performance characteristics obtained for a PPLN SPOPO operating with a BF in the 1.8 μm region, with pulse duration of ~4 ps. First, we compare the advantages and disadvantages of a diffraction grating and a birefringent filter in a SPOPO context. We then outline the basic characteristics of BFs and the particular design approach for BFs suitable for use in SPOPOs. We conclude with a description of the performance achieved with a custom-built BF based on this design approach.

An important consideration in the use of a diffraction grating as an OPO 'mirror' (see Ref. 2 for a detailed discussion of a retro-reflecting, Littrow arrangement) is the significant insertion loss. Two contributions to this loss, namely, the basic efficiency of the grating, and the loss (specific to synchronously pumped, i.e. short-pulse operation) due to the introduction of pulse tilt via the action of the grating [2], are avoided with the BF. Thus, very much lower insertion losses can be achieved with the BF compared to the overall ~30% loss observed with the grating [2]. Like the grating, the BF introduces some inevitable loss for pulsed operation, arising from the spectral attenuation associated with its filter action and also, from the fact that

the spectrally narrowed, and consequently temporally broadened, pulse overlaps less well with the pump pulse. We will provide estimates of these losses, noting that some compromise needs to be made between the benefit of filtering and its inevitable consequence of loss. The reduced loss compared to the grating is a significant benefit, suggesting that a BF could be used in low-gain SPOPOs (e.g. based on LBO as the nonlinear medium), or even in cw-pumped OPOs. It is also worth noting that a low-loss BF would be suited for SPOPO operation at very long idler wavelengths for which it is important to keep signal losses as low as possible [6,7]. Another advantage that the BF can have over the grating is the ease of alignment, avoiding the stringent requirement for the grating that, for wide tuning, the rotation axis of the grating needs to be accurately aligned to the grating grooves and accurately perpendicular to the incident signal beam.

On the other hand the grating has the considerable benefit that the spectrum of retro-reflected light can have a single maximum, and hence it is not constrained by free-spectral-range limitations associated with the channeled spectrum of a BF. In fact, the BF not only has the channeled spectrum of its main transmission peaks, but there are also the multiple intervening subsidiary transmission maxima. This problem is particularly relevant in the usual BF designs which rely on Brewster-angle orientation of its faces to provide the polarization discrimination. While these designs have an attractively low loss at the main transmission peaks, the weak polarization discrimination of the Brewster surfaces allows subsidiary maxima to have significant transmission. Of course, in the case of low-gain oscillators (e.g. for cw-pumped Ti:sapphire lasers), the presence of these subsidiary maxima using standard commercial BFs need not present a problem since even their significant transmission (e.g. >80%) may be too low to allow oscillation under low-gain conditions. However, in the case of a SPOPO, very

substantial parametric gains can be produced (typically, many dB) and unless the transmission of the subsidiary maxima is strongly suppressed, the OPO will suffer a restricted tuning range if, during tuning via the BF, the signal oscillation can jump to the frequency of a subsidiary transmission maximum.

2. Basic characteristics of Birefringent filters

The need to strongly suppress the subsidiary maxima of a BF has previously been addressed [8] in the context of a high-gain dye laser, using a four-plate BF with plate thickness in the ratio 1:2:4:8. We have adopted this same thickness ratio in our design (although designed for longer wavelengths, ~1.8 μm, and different free-spectral-range) and confirm, both by calculation and experiment, that it can provide extensive signal tuning ranges across the parametric gain profile before a signal jump to a subsidiary peak occurs. Before describing this design in detail we first recapitulate some of the main design features of such a Brewster-orientated, multi-plate BF. A more detailed discussion can be found in Ref. 9. We shall consider the particular design [8] consisting of four quartz plates, of thickness ratio 1:2:4:8 each with its optic axis lying in the face of the plate and all the axes aligned parallel and so maintained while the plates are rotated as a unit about the axis N (normal to the plate, see Fig. 1). Light is incident at Brewster's angle (horizontal plane of incidence) and the orientation of the optic axis is specified by the angle φ between the optic axis OA and the horizontal (labeled P in Fig. 1, corresponding to the E-field direction of the p polarization). With this arrangement, p-polarized light, at (vacuum) wavelength λ, incident at Brewster's angle will exit as p-polarized light, hence without loss, provided λ satisfies

$$\frac{2\pi(n'_e - n_o)L_1}{\lambda} = 2\pi N_1, \qquad (1)$$

where N_1 is an integer and L_1 is the physical path length of the refracted ray inside the thinnest plate. Here, the symbol n'_e, denotes the extraordinary index experienced by the propagating light inside the crystal (different from the usual extraordinary refractive index, n_e, defined for light propagating perpendicular to the optic axis, since in general the angle between propagation direction and the optic axis, which depends on θ and φ, is less than 90°). Automatically, this same relationship is satisfied for the other plates (with integers increased by factors of two in accordance with the ratio of their thicknesses). The corresponding transmission peaks for the BF have 100% transmission. There will be a number of such 100% transmissions, which we refer to as the main transmission peaks. Thus, the frequency spacing, $\Delta\nu_{FSR}$, between adjacent main transmission peaks (the free-spectral-range) is

$$\Delta\nu_{FSR} = \frac{c}{(n'_e - n_o)L_1}. \qquad (2)$$

The spectral width of the transmission peak is predominantly determined by the thickness of the thickest plate. This spectral width needs to be selected to be wide enough to provide high transmission for the signal spectrum, but narrow enough to enforce the desired frequency tuning/filtering. As the plates are rotated (φ in Fig. 1 is varied), so the extraordinary index, n'_e, changes and so the wavelength of the main transmission peak, determined by Eq. (1), is altered. Between these main transmission maxima, there are subsidiary maxima. These maxima would exhibit strongly reduced transmission if polarizers were situated between each plate, to eliminate the s polarization, and their spectral positions would then roughly correspond to the full-wave plate condition being satisfied for plates other than the thinnest plate. But the presence of the polarizers would introduce additional unwanted loss and imply a more complicated design than that which simply uses the Brewster surfaces to act as the (imperfect) polarization discriminators.

Thus, the price paid for a simple, low-loss, device is a significant transmission on the subsidiary maxima. We also note that the positions of these subsidiary maxima no longer correspond in general to the full-wave plate condition of the various plates. As the filter is rotated so the precise pattern of the subsidiary maxima changes (the height and position) since for a given input polarization the relative split between e and o components changes with φ, and the incomplete removal of the s-polarized component at the output face of a plate, then allows this component into the next plate. The presence of these subsidiary maxima need not be troublesome in a low-gain oscillator, but to achieve wide tuning in a high-gain oscillator it is necessary to design the BF to help suppress these maxima. This is the basis of the 1:2:4:8 design, described in Ref. 8.

3. Birefringent filter design for use in a SPOPO

After this brief survey of the general principles of the BF design, we now emphasize the particular features that are relevant to the SPOPO. First, we need to consider the appropriate thickness of the thick plate. This determines the width of the main transmission peak, and hence the magnitude of the loss, due to its filter-action on the spectrum of the incident pulse. Then we consider the question of the actual tuning range, which will in general be significantly less than the free-spectral-range defined in Eq. (2), since frequency hopping to subsidiary maxima may, in fact, determine the range. Thus, as one tunes the main transmission peak away from the peak of the parametric gain, the situation may occur that the net gain on a subsidiary maximum closer to the gain peak, exceeds that on the main transmission peak of the BF. Oscillation will then jump to the subsidiary maximum. In discussing this question we shall make some numerical estimates of expected performance.

A rough estimate of the bandwidth of the main BF transmission peak, is found by considering a Lyot filter of birefringence $n'_e - n_o$, and of thickness equal to the path length, L_4, in the thick plate. The power transmission of such a filter has the form

$$\cos^2\left(\frac{\pi(n'_e - n_o)L_4 \nu}{c}\right). \tag{3}$$

Thus, the spectral width (FWHM) of the transmission intensity is $c/2(n'_e - n_o)L_4$. In practice, the actual FWHM will be slightly different from this, say $xc/2(n'_e - n_o)L_4$, where $x \sim 1$, due to the fact that the transmission involves the combined effect of the overlapping maxima of four plates and is also modified by the fact that, unlike the ideal Lyot filter, the s polarization is not totally rejected. The actual value of x, obtained from numerical calculations for our 1:2:4:8 design, is ~0.6 when $\varphi \sim 40°$. This value of x will be included in our calculations.

For convenience in making estimates of the integrated transmission across the finite spectrum of an incident pulse, we simulate the $\cos^2$ function above by a Gaussian transmission function having the same FWHM power transmission. This has the form, for power transmission $T(\nu - \nu_0)$, around a transmission peak at ν_0,

$$T(\nu - \nu_0) = \exp\left(\frac{-(\nu - \nu_0)^2 16(n'_e - n_o)^2 L_4^2 \ln 2}{c^2 x^2}\right) \tag{4}$$

$$= \exp\left(\frac{-(\nu - \nu_o)^2}{(\Delta\nu_{BF})^2}\right),$$

where

$$(\Delta\nu_{BF})^2 \equiv x^2 c^2 / \left[16\ln 2 (n'_e - n_o)^2 L_4^2\right].$$

Now we consider the effect on the power transmission of an incident pulse, with spectral width $\Delta\nu_S$, whose power spectrum is given by $\exp\left\{-\left[(\nu - \nu_0)/\Delta\nu_S\right]^2\right\}$. The resultant

transmission is $\left[1+(\Delta\nu_S/\Delta\nu_{BF})^2\right]^{-1/2}$, and thus, for a small spectral width of the pulse, i.e. $\Delta\nu_S << \Delta\nu_{BF}$, the power loss is $\sim(\Delta\nu_S/\Delta\nu_{BF})^2/2$. For our signal pulses, of duration FWHM τ = 4 ps, hence spectral width FWHM = $0.44/\tau = 2(ln2)^{1/2}\Delta\nu_S$, one has a loss $\sim\left\{0.4\left[(n'_e - n_o)L_4/\tau c\right]^2\right\}$, which for our design implies less than 1% per round trip of the oscillator.

The calculation of effective loss can be further refined, if so desired, by considering the temporal broadening of the pulse due to the spectral narrowing, with the consequent reduced overlap with the pump pulse, and hence reduced parametric gain. The bandwidth of the transmitted pulse, $\Delta\nu_T$, is related to that of the incident pulse via $(\Delta\nu_T)^{-2} = (\Delta\nu_S)^{-2} + (\Delta\nu_{BF})^{-2}$, and the fractional decrease in bandwidth for the case $\Delta\nu_S << \Delta\nu_{BF}$ is $(\Delta\nu_S/\Delta\nu_{BF})^2/2$. The small increase in pulse width which is implied for our operating condition can be safely neglected. There is in fact an additional broadening due to the fact that the BF introduces a frequency dependent phase shift and hence a chirp on the transmitted pulse. This is also small for the parameters of our design and is neglected here.

We now elaborate further on our design choice of plate thickness, i.e. 12 mm for the thick plate. The corresponding transmission bandwidth is more than adequate for our 4-ps pulses and the thickness could have been greater without introducing significant loss. The total path length for a double pass through the entire BF, is ~54 mm. The dispersion length given by $L_D = \tau^2/\left\{4\ln 2\left[d(1/v_g)/d\omega\right]\right\}$ [10] where v_g is the group velocity, is ~80 m, for our 4-ps pulses at 1.8 μm, hence much greater than the physical path length in the BF. This implies that the effect of GVD from this length is still acceptably small and greater thickness could be tolerated. So, in fact the upper limit of thickness of plates was chosen mainly on the grounds of convenient compactness. On the other hand, there is a more compelling reason for not using a much shorter

length, in addition to the obvious requirement that the BF should exert a significant filtering action and give adequate frequency selection to provide robust control over the tuning behavior. This reason has to do with the extent of the tuning range that can be covered by tuning the transmission peak of the BF (i.e. by changing angle φ).

The thickness of the thinnest plate determines the free-spectral-range, i.e. the frequency separation between the main transmission peaks. The frequency corresponding to a transmission maximum is tuned by rotating the BF, i.e. changing the angle φ. The frequency range over which such a maximum can be tuned is ultimately limited by the maximum range of φ, i.e. 90°. Of course, at the limits of this range, where $\varphi = 0$ or 90°, the incident light (assumed to be p polarized) will have either just an ordinary or just an extraordinary component, and in either case the device ceases to operate as a wave-plate. The transmission is then independent of wavelength and no filter action occurs. In fact, as the angle φ moves progressively away from ~40°, where incident p-polarized light has equal e and o components inside the plate, the heights of the subsidiary maxima progressively rise relative to the main transmission peaks. Thus, the usefulness of the BF, in so far as it depends on an adequate suppression of the side maxima, diminishes as one rotates away from φ ~40°. The design aspect that we have borne in mind is that if the entire spectral region is to be accessed with the one BF, one needs the free-spectral-range small enough so that one can tune over this range with a small enough change of φ to ensure that subsidiary maxima remain sufficiently low.

4. Calculation of Birefringent filter transmission characteristics

To check the height of these subsidiary maxima and their dependence on φ, a detailed calculation is needed of the BF transmission characteristics. To do this we have made use of the analysis of Preuss and Cole [9], on which Zagone and Hetherington [8] also based their analysis. We adopt

the notation used by Zagone and Hetherington. Details of the analysis are given in Appendix A, where for clarity we restate the relevant equations having removed typographical errors that appear in both of these papers.

In considering the filter characteristics shown by the BF when inserted into the OPO resonator, it needs to be appreciated that the behaviour is modified from the transmission behaviour of the filter on its own. This is because the gain medium has a polarization discrimination resulting from, in our case, the PPLN crystal providing gain only for the p polarization (the crystal is oriented to give maximum gain for the polarization, parallel to its z-axis, for which the filter has maximum transmission, i.e. p). The s polarization experiences no gain, nor is it attenuated by the crystal, and is then returned to the BF along with the amplified p polarization.

Thus in general, rather than simply considering the transmission of the BF for the p-polarized component, one needs to consider the eigenpolarization of the resonator, i.e. the polarization state that is reproduced after a round-trip, having undergone changes of polarization state due to the separate effects of the BF and the nonlinear medium. This eigenpolarization therefore depends on the parametric gain. The effect of this gain-induced polarization discrimination is basically the same as would result from adding, after the BF, an analyzer with the same degree of polarization discrimination. A comparison of the overall filter characteristics with varying degrees of this polarization discrimination (shown below), indicate that the ratio between the transmitted intensities of the main transmission peak and its neighboring subsidiary peaks can be significantly affected by this polarization discrimination, and the depth of the transmission minima is altered. We have also included in the analysis, the spectral behavior of the parametric gain profile, and, in the numerical calculations, have used the values of parametric

gain and bandwidth that match those of the experimental conditions employed in our testing of the BF performance. This has then allowed, via calculation of the net round-trip gain as a function of frequency, to predict when, as the main filter peak is tuned across the gain profile, a jump of oscillation frequency to a subsidiary filter peak will occur. Therefore, one can predict the extent of tuning achievable across the parametric gain profile.

Thus our calculations (fully derived in Appendix A) have taken the following form. A general polarization state, represented by a Jones vector $\begin{bmatrix} E_S^{in}(\omega) \\ E_P^{in}(\omega) \end{bmatrix}$, is incident on a single birefringent filter, and undergoes a change of polarization state, due to the different transmission t_S, t_P at the Brewster face. Then, the wave-plate action is described by a Jones matrix $\begin{pmatrix} ss & sp \\ ps & pp \end{pmatrix}$ after which there is again s, p discrimination resulting from transmission through the output Brewster face. This process of calculation is repeated for each plate in succession giving an overall Jones matrix for the BF of $\begin{pmatrix} SS & SP \\ PS & PP \end{pmatrix}$. Note that this transformation includes the double-pass incurred by the BF due to the standing wave resonator configuration (i.e. output fields after the first transit of the four-plate BF being then reflected back through the plates again). The output, $\begin{bmatrix} E_S^{4\ plate}(\omega) \\ E_P^{4\ plate}(\omega) \end{bmatrix}$, leaving the BF at this stage then undergoes parametric gain in the nonlinear crystal (multiplicative power gain $G(\omega)$ for the p polarization, unity gain for the s polarization), resulting in fields given by

$$\begin{bmatrix} E_S^{out}(\omega) \\ E_P^{out}(\omega) \end{bmatrix} = \begin{pmatrix} r_S & 0 \\ 0 & r_P\sqrt{G(\omega)} \end{pmatrix} \begin{bmatrix} E_S^{4plate}(\omega) \\ E_P^{4plate}(\omega) \end{bmatrix} = \begin{pmatrix} r_S & 0 \\ 0 & r_P\sqrt{G(\omega)} \end{pmatrix} \begin{pmatrix} SS & SP \\ PS & PP \end{pmatrix} \begin{bmatrix} E_S^{in} \\ E_P^{in} \end{bmatrix}. \qquad (5)$$

Here r_S, r_P represent the effective amplitude reflection coefficients for s and p (in general not equal) to account for additional resonator losses (eg. an output coupler) which may be polarization-dependent (if for example an additional polarizing element is added). The eigenpolarization satifies the condition of an unchanged polarization state after a round trip, i.e.

$$\begin{bmatrix} E_S^{out}(\omega) \\ E_P^{out}(\omega) \end{bmatrix} = \gamma(\omega) \begin{bmatrix} E_S^{in}(\omega) \\ E_P^{in}(\omega) \end{bmatrix}. \qquad (6)$$

The growth per round-trip of the intracavity signal intensity is then given by $|\gamma(\omega)|^2$. Details of the procedure for calculating $\gamma(\omega)$ which involve a quadratic equation for γ obtained by substituting the two equations from Eq. (6) into Eq. (5), are given in Appendix A. This completes the description of the general procedure for calculating the filter transmission characteristics, apart from the detail of how the parametric gain profile is calculated. Before considering that, we first examine the predicted behavior as the filter is tuned by changing φ. For these calculations we have assumed a constant $G(\omega)$, i.e. independent of ω, and have plotted the signal intensity gain normalized to unity for the main peaks. The effect of the presence of G in the calculation is then simply to add a polarization (intensity) discrimination for the p polarization over the s polarization, equivalent to adding an analyzer with this degree of discrimination. Comparison of Figs 2a, b and c shows the effect of three different G values, respectively $G = 1, 5, 40$. Note that the relative height of the maxima is significantly changed by adding a modest discrimination ($G = 5$), suggesting that the introduction of an additional polarizing element could be worthwhile. Increasing G beyond 40 had little further effect, and the results of other calculations shown here will all be for $G = 40$, this corresponding to the small-signal parametric gain of our experimental set-up. The general effect of changing φ is shown in Fig. 3, (peak transmission, at ν_0 = 172 THz, normalized to unity). At the main

transmission maximum, corresponding to each plate being a full-wave plate, the polarization remains p at each Brewster face of the BF and throughout the resonator, thus the BF actually has unity transmission. Fig. 3a shows a free-spectral-range ($\Delta\nu_{FSR}$), between main transmission maxima of ~40 THz, i.e. ~310 nm when one peak is set at 1750 nm (ν_0 = 172 THz). This spectrum corresponds to φ = 40°, at which the heights of the subsidiary maxima are most strongly suppressed since this corresponds to equal e and o components inside the plates (more generally the angle φ for which this occurs is given by $\varphi = \cos^{-1}\left[\left(2-\left(\sin^2\theta/n^2\right)\right)^{-1/2}\right]$, which for quartz gives $\varphi \sim 40°$. Figs. 3b and c show the effect of changing φ (to 23° and 58° respectively) to tune the main maximum to the mid-point of the free-spectral-range. In each case in Figs. 3b and c one can see the increase in height of the subsidiary maxima as φ departs significantly from ~40°. Nevertheless, over the angle range of φ from 23° to 58° this degradation in frequency selectivity is not severe and indicates that this design should allow satisfactory tuning over each free-spectral-range (e.g. that between the maxima at 1750 nm (172 THz) and 1450 nm (207 THz) and so on for the other maxima). This design would therefore allow coverage of the entire spectrum.

5. Calculation of tuning range

We now examine the effect of the subsidiary maxima in limiting the tuning range as the OPO is tuned across the parametric gain profile. We consider the situation of a specific peak parametric gain, over a crystal length l, assuming plane-wave conditions, and an undepleted pump: Exact phase-matching, $\Delta k = 0$, corresponds to the peak ($\omega = \omega_0$) of the gain curve i.e. $G(\Gamma, \Delta k = 0) = \cosh^2(\Gamma l)$. Where $\Gamma = N^{1/2}\Gamma_{th}$ is the parametric gain coefficient for operation at a

pump intensity N times the threshold intensity and Γ_{th} is experimentally determined as previously described in Ref. 2. The parametric gain is then calculated at a frequency ω shifted from the peak at ω_0 by $\Delta\omega = \omega - \omega_0$ (for which there is a corresponding phase-mismatch $\Delta k(\Delta\omega)$), using [see Ref. 2]

$$G(\Gamma, \Delta k(\Delta\omega)) = 1 + \frac{\Gamma^2 \sinh^2(gl)}{g^2}, \tag{7}$$

where

$$g(\Gamma, \Delta k(\Delta\omega)) = \sqrt{\Gamma^2 - \left(\Delta k(\Delta\omega)/2\right)^2}.$$

We then calculate $|\gamma(\omega)|^2$ having substituted $G(\Gamma,\Delta k(\Delta\omega))$ from Eq. (7) for $G(\omega)$ in Eq. (5). The value of $G(\Gamma,\Delta k=0)$ in these calculations is taken to be 40 (~16 dB) and Fig. 4 shows the corresponding value of $|\gamma|^2$, i.e. the small-signal power gain per round-trip as a function of wavelength λ. $\Delta k(\Delta\omega)$ is calculated using the Sellmeier equations for lithium niobate [11] with a PPLN period chosen to give peak signal gain at 1800 nm for a 1047 nm pump. The lowest threshold will be for the wavelength at which net gain is greatest and it is assumed that oscillation will take place at this wavelength. Figs. 4b and c show the net round-trip gain as the main filter peak is tuned to longer wavelengths from the 1800 nm peak, by changing φ. It can be seen in Fig. 4c that a frequency jump to a subsidiary maximum can be expected to occur when the signal wave is tuned to ~1818 nm. One should also note that when oscillation occurs on the subsidiary maximum, the corresponding eigenpolarization has some s component (since the matrix element sp is nonzero), which would be readily observed in the output, whereas for oscillation on the main transmission peak the polarization remains p. Thus, this calculation gives a quantitative demonstration of the expected frequency hopping to a subsidiary maximum. We

also note that the particular circumstances corresponding to this calculation indicate a total tuning range of ~35 nm, representing a significant coverage of the parametric gain profile (~33 nm, FWHM). The benefit of strong suppression of the subsidiary maxima is clearly evident.

6. Experimental Results

The OPO investigated in this work is configured as a standing-wave resonator (see Fig. 5). A single PPLN crystal of length 19 mm with a period of 28.5 μm, held at a temperature of 130 °C, and pumped at a wavelength of 1047 nm resulted in a phase-matched signal wavelength of ~1820 nm. We note here that the temperature-dependent Sellmeier equation described in Ref. 11 was used to define the PPLN refractive indices for all results presented in this work. The pump source, an additive-pulse mode-locked Nd:YLF laser (Microlase DPM-1000-120, λ = 1047 nm), provides a train of 4-ps pulses at 120 MHz, which is coupled into a Q-Peak amplifier module (MPS-1047 CW-10 with output coupler removed), used in a double-pass configuration, to deliver up to 3.5 W of average pump power to the PPLN crystal. M^2 values for the pump beam were measured to be ~1.05, indicating that the amplifier caused negligible degradation in beam quality. Likewise, changes in spectral shape and pulse duration were also negligible. The pump beam is focused to a spot-size of 48 μm at the centre of the PPLN crystal; the pump focusing parameter ξ_p (ratio of crystal length to pump confocal parameter) was calculated to be 0.6. The curved mirrors in the cavity (radius of curvature = 200 mm) define a spot-size for the resonated signal of 55 μm. The corresponding signal focusing parameter, ξ_s, is 0.70.

A custom-built, four-plate birefringent filter [12] with plate thicknesses of 1.5 mm, 3 mm, 6 mm and 12 mm made to thickness tolerances of ±2 μm was inserted in one of the arms

of the SPOPO as shown in Fig. 5. The filter plates were mounted at Brewster's angle resulting in a small translation but no angular deviation in the transmitted laser beam. The signal spot-size at the location of the BF was ~0.9 mm. To allow for the additional optical path through a double-pass of the quartz BF, the round-trip cavity length was shortened, relative to the empty cavity, by ~31 mm by simple translation of mirror A (see Fig. 5) to maintain synchronism between the signal and pump pulses. The output coupler reflectivity used in this experiment was 50% for the signal. The average power threshold, incident on the PPLN crystal, measured for the SPOPO with the BF tuned to the peak of the gain curve at 1822 nm was 560 mW. With the BF removed from the cavity an oscillation threshold of 520 mW was obtained. We ascribe this threshold change to a small degree of beam clipping within the BF as the aperture dimension was rather close to the beam-width. Using the BF, with an average pump power of 3.5 W incident on the PPLN crystal, a maximum signal output power of 1.15 W at 1822 nm was recorded, corresponding to a signal conversion efficiency of 33%. Under these experimental conditions we measured (using the technique described in Ref. 2) a single-pass, small-signal gain of ~40. Fig. 6a displays the tuning curve obtained by simple rotation of the BF. Fig. 6b shows the rotation angle required to obtain a particular signal wavelength. The frequency jump to a subsidiary maximum that occurs at either end of the tuning range is also shown. The observed tuning rate of ~0.5 nm/mrad agrees well with the predictions derived from Fig. 4. It was confirmed that the output polarization contained a substantial s component when oscillation occurred on the subsidiary peaks, but was essentially a pure p component over the 30 nm range covered by the main peak. The extent of this tuning range was slightly less than the calculated 35 nm (see Fig. 4 and the corresponding discussion in the text). A possible explanation for this lies in the assumed value of parametric gain (40x) used in our calculations. In fact, it could be argued that the

appropriate gain to use is that which corresponds to the saturated gain resulting from the depleted pump. Given the output coupler transmission, combined with other losses in the resonator this would correspond to a saturated gain of ~3. However, under these conditions of pump depletion one can no longer use the parametric gain expression of Eq. (7) in order to calculate the tuning range. We note, however, from Fig 2b, that with an assumed parametric gain of 5, the discrimination between main peaks and subsidiary peaks is reduced from that for $G = 40$, and this would therefore be expected to reduce the available tuning range. This could explain the ~15% discrepancy between our calculated and observed ranges. So, the inclusion of an additional polarizing element, to enhance the discrimination of p over s, could give a useful increase of the tuning range. A relatively simple element, such as a Brewster plate should serve this purpose (e.g. Zinc Selenide plate, with a refractive index of ~2.5 would give a further factor of 4 intensity discrimination).

Finally we note that the inclusion of the BF has the beneficial effect, as observed with the use of the diffraction grating, of reducing the tendency for the OPO to generate extra spectral content when operated many times above threshold. Fig. 7 shows an example of this behavior. With no BF and with the PPLN crystal temperature tuned to provide signal oscillation at 1824 nm it is found that for pumping up to ~5 times threshold the signal output consists of a single line at 1824 nm. For higher levels above threshold additional lines appear and can actually contain more power than the 1824 nm line, as shown in the figure for ~8 times threshold. With the BF inserted, tuned to 1824 nm, and operating under the same conditions the spectrum again became a single line at 1824 nm, as shown in Fig. 7.

7. Conclusions

We have considered the use of a birefringent filter as a tuning element in a synchronously pumped OPO, indicating the general design principles that influence the tuning range that can be achieved with such a device. An important design consideration has been the need to enhance the selectivity of the main transmission peak of the BF, relative to the subsidiary transmission maxima in order to maximize the tuning range. For this reason we have adopted a 4-plate design; with plate thicknesses in the ratio 1:2:4:8. Calculations of the transmission characteristics of this filter have been made, leading to the conclusion that it should provide satisfactory tuning characteristics across each free-spectral-range. Experimentally observed tuning across the parametric gain bandwidth provided by a PPLN SPOPO operating around 1800 nm confirmed that tuning covered a substantial part of the gain bandwidth before a frequency hop to a subsidiary transmission maximum occurred. Extension of this tuning should be possible by introducing some additional polarization discrimination, for example in the form of a separate plate oriented at Brewster's angle. We also confirmed that this BF was effective in suppressing the generation of extra spectral features when operated many times above threshold. This same design, with the same dimensions should work satisfactorily with somewhat shorter pulses, down to ~1 ps, before the loss due to its filter action becomes significant. For yet shorter pulses one could, in principle, scale down the plate thicknesses, but this is likely to raise practical problems with the thinnest plate. Since it may be of interest to others to explore other parameter ranges, including the use of different nonlinear media, different output coupling values etc, we have aimed at giving a sufficiently full description of the design philosophy and calculation procedure that it will make further exploration a straightforward matter.

8. Acknowledgements

This work has been supported by the UK Engineering and Physical Sciences Research Council (EPSRC). Malcolm Watson acknowledges the support of an EPSRC studentship. Martin O'Connor's email address is moc@orc.soton.ac.uk.

9. Appendix A

A.1 Sellmeier equation for Quartz [13].

Ordinary refractive index

$A_o = 1.28604141$, $B_o = 1.07044083$, $C_o = 1.00585997\text{E-}2$, $D_o = 1.10202242$, $F_o = 100$

Extraordinary refractive index

$A_e = 1.28851804$, $B_e = 1.09509924$, $C_e = 1.02101864\text{E-}2$, $D_e = 1.15662475$, $F_e = 100$

$$n_{o/e}(\lambda) = \sqrt{A_{o/e} + \frac{B_{o/e}\lambda^2}{(\lambda^2 - C_{o/e})} + \frac{D_{o/e}\lambda^2}{(\lambda^2 - F_{o/e})}}. \qquad \text{(A1)}$$

A.2 Calculation of Eigenpolarization via Jones calculus.

The polarization transformation due to a single birefringent plate, tilted and rotated with respect to the input beam axes as shown in Fig. 1, and including the transmission at the plate surfaces is given in terms of Jones matrices by

$$\begin{bmatrix} E_S^{1\,plate}(\omega) \\ E_P^{1\,plate}(\omega) \end{bmatrix} = \begin{pmatrix} t_S & 0 \\ 0 & t_P \end{pmatrix} \begin{pmatrix} ss & sp \\ ps & pp \end{pmatrix} \begin{pmatrix} t_S & 0 \\ 0 & t_P \end{pmatrix} \begin{bmatrix} E_S^{in} \\ E_P^{in} \end{bmatrix}, \qquad \text{(A2)}$$

where the frequency dependence of the output fields is indicated explicitly, arising from the frequency dependence of the matrix elements ss, sp etc. The elements are given by

$$ss = \frac{\exp(\imath\delta_e)(n_o^2 - \sin^2\theta)\cos^2\varphi + \exp(\imath\delta_o)n_o^2\sin^2\varphi}{(n_o^2 - \cos^2\varphi\sin^2\theta)} \qquad \text{(A3)}$$

i.e. the amplitude of incident s preserved as s.

$$pp = \frac{\exp(\iota\delta_o)(n_o^2 - \sin^2\theta)\cos^2\varphi + \exp(\iota\delta_e)n_o^2\sin^2\varphi}{(n_o^2 - \cos^2\varphi\sin^2\theta)} \tag{A4}$$

is the amplitude of incident p preserved as p, and

$$sp = ps = \frac{[\exp(\iota\delta_e) - \exp(\iota\delta_o)](n_o\sin\varphi\cos\varphi)(n_o^2 - \sin^2\theta)^{1/2}}{(n_o^2 - \cos^2\varphi\sin^2\theta)} \tag{A5}$$

is the amplitude of incident p/s transformed to s/p. t_S and t_P represent the amplitude transmission coefficients of the plate surface for the s and p polarization, respectively. The phases of the field components along the extraordinary and ordinary directions are

$$\delta_e = 2\pi n_e t\bar{\nu}\frac{\left[1 + \sin^2\theta\cos^2\varphi\left(\frac{1}{n_e^2} - \frac{1}{n_o^2}\right)\right]}{\left[1 - \sin^2\theta\left(\frac{\sin^2\varphi}{n_e^2} + \frac{\cos^2\varphi}{n_o^2}\right)\right]^{1/2}}, \tag{A6}$$

$$\delta_o = 2\pi n_o t\bar{\nu}\left(1 - \frac{\sin^2\theta}{n_o^2}\right)^{-1/2}, \tag{A7}$$

where t is the thickness and $\bar{\nu}$ is the frequency in cm^{-1}.

This transformation is then successively repeated to obtain the overall signal field transformation for a double-pass through the four-plate BF

$$\begin{bmatrix} E_S^{4\ plate} \\ E_P^{4\ plate} \end{bmatrix} = \begin{pmatrix} SS & SP \\ PS & PP \end{pmatrix}\begin{bmatrix} E_S^{in} \\ E_P^{in} \end{bmatrix}, \tag{A8}$$

where SS, SP, PS and PP are the elements for the overall transformation between the s and p polarizations for the four-plate BF in the double-pass configuration. It is important to note here that for the return pass through the BF the angle φ changes sign and the direction of the axis P and the surface normal must also be reversed to restore a right handed basis set. These changes

result in a Jones matrix for the return pass which is identical to the first pass but with the order of the plates reversed.

The intracavity signal field leaving the BF then undergoes gain in the nonlinear crystal (multiplicative power gain $G(\omega)$ for the p polarization, unity gain for the s polarization). Therefore, the eigenpolarization, which satisfies the condition that the same polarization state is reproduced after a round-trip, is given by

$$\begin{bmatrix} E_S^{out}(\omega) \\ E_P^{out}(\omega) \end{bmatrix} = \begin{pmatrix} r_S & 0 \\ 0 & r_P\sqrt{G(\omega)} \end{pmatrix} \begin{bmatrix} E_S^{4\,plate}(\omega) \\ E_P^{4\,plate}(\omega) \end{bmatrix} = \begin{pmatrix} r_S & 0 \\ 0 & r_P\sqrt{G(\omega)} \end{pmatrix} \begin{pmatrix} SS & SP \\ PS & PP \end{pmatrix} \begin{bmatrix} E_S^{in} \\ E_P^{in} \end{bmatrix}. \qquad \text{(A9)}$$

The condition for the field to be an eigenpolarization is $E_{S,P}^{out} = \gamma(\omega) E_{S,P}^{in}$, where $\gamma(\omega)$ represents the net gain of the E-field amplitude per round-trip. So (with $r_S = r_P = r$, for simplicity),

$$\gamma E_P^{in} = r\sqrt{G(\omega)}\left(PPE_P^{in} + PSE_S^{in}\right). \qquad \text{(A10)}$$

Also, for an eigenpolarization, we must have the same growth for E_S, i.e. $E_S^{out} = \gamma(\omega) E_S^{in}$. So,

$$\gamma E_S^{in} = r\left(SSE_S^{in} + SPE_P^{in}\right). \qquad \text{(A11)}$$

Substituting E_S^{in} from Eq. (A11) into Eq. (A10) the resulting quadratic equation,

$$\gamma^2 - \left(rSS + r\sqrt{G}PP\right)\gamma - r^2\sqrt{G}\left(SP.PS - PP.SS\right) = 0, \qquad \text{(A12)}$$

can be solved for γ. Therefore, the growth per round-trip of the intracavity signal intensity is given by $|\gamma(\omega)|^2$.

References

1. K. Puech, L. Lefort, and D. C. Hanna: J. Opt. Soc. Am. B **16**, 1533 (1999). Also refer to errata J. Opt. Soc. Am. B **17**, 1102 (2000).
2. D. C. Hanna, M. V. O'Connor, M. A. Watson and D. P. Shepherd: J. Phys. D: Appl. Phys. **34**, 2440 (2001).
3. M. Ebrahimzadeh, P. J. Phillips, S. Das: Appl. Phys. B **72**, 793 (2001).
4. M. A. Watson, M. V. O'Connor, D. P. Shepherd, and D. C. Hanna: Opt. Lett. **28** (20) 1957 (2003).
5. T. W. Tukker, C. Otto, and J. Greve: J. Opt. Soc. Am. B **16** (1) 90 (1999).
6. L. Lefort, K. Puech, G. W. Ross, Y. P. Svirko, and D. C. Hanna: Appl. Phys. Lett. **73**, 1610 (1998).
7. M. A. Watson, M. V. O'Connor, P. S. Lloyd, D. P. Shepherd, D. C. Hanna, C. B. E. Gawith, L. Ming, P. G. R. Smith, O. Balachninaite: Opt. Lett. **27** (23), 2106 (2002).
8. R. L. Zagone and W. M. Hetherington 3rd: Appl. Opt. **35** (4), 624 (1996).
9. D. R. Preuss and J. L. Gole: Appl. Opt. **19** (5), 702 (1980).
10. O. Svelto: *Principles of Lasers*, 4th edition (Plenum, New York 1998).
11. D. H. Jundt: Opt. Lett. **22** (20), 1553 (1997).
12. IC Optical Systems Ltd UK, http://www.icopticalsystems.com/index.html.
13. G. Ghosh: Opt. Commun. **163**, 95 (1999).

Figure Captions

Fig. 1. OA is the optic axis and is in the plane of the birefringent filter face, axes S and P lie in the face, are mutually orthogonal and S is perpendicular to the plane of incidence. The angle of incidence, θ, (measured from the axis N which is normal to the plate surface) is set to Brewster's angle. The angle φ indicates the rotation of the optic axis from the P axis.

Fig. 2. Signal intensity gain (normalized) as a function of frequency for different G values ($\varphi =$ 40°) **a** $G = 1$, **b** $G = 5$, **c** $G = 40$.

Fig. 3. Signal intensity gain (normalized) as a function of frequency (* transmission maximum tuning): **a** $\varphi = 40°$, **b** $\varphi = 23°$, **c** $\varphi = 58°$.

Fig. 4. Net small-signal power gain per round-trip, ($|\gamma|^2$), as a function of wavelength (including output coupling reflection coefficients: $r_S = r_P = \sqrt{0.5}$): **a** $\varphi = 45.6°$, **b** $\varphi = 46.5°$, **c** $\varphi = 47.5°$.

Fig. 5. Schematic of the optical parametric oscillator: OC- output coupler; BF- 4-plate birefringent filter; PPLN- periodically poled lithium niobate crystal; A- back mirror used to resynchronize cavity length.

Fig. 6. **a** Signal output power and **b** Birefringent filter rotation angle as a function of wavelength; central tuning peak (filled diamonds), subsidiary maximum tuning peak (unfilled diamonds).

Fig. 7. Typical signal output spectrum with and without the intracavity birefringent filter.

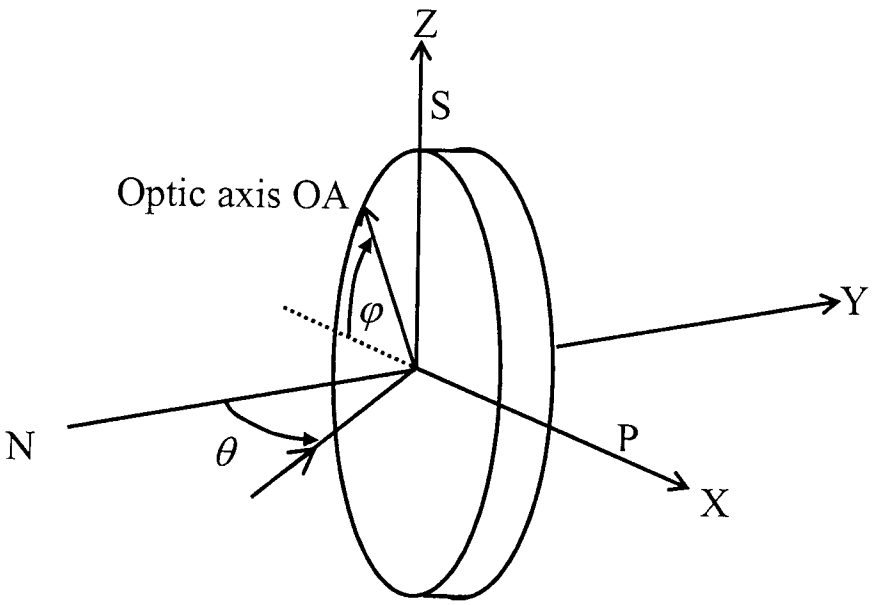

Fig. 1. OA is the optic axis and is in the plane of the birefringent filter face, axes S and P lie in the face, are mutually orthogonal and S is perpendicular to the plane of incidence. The angle of incidence, θ, (measured from the axis N which is normal to the plate surface) is set to Brewster's angle. The angle φ indicates the rotation of the optic axis from the P axis.

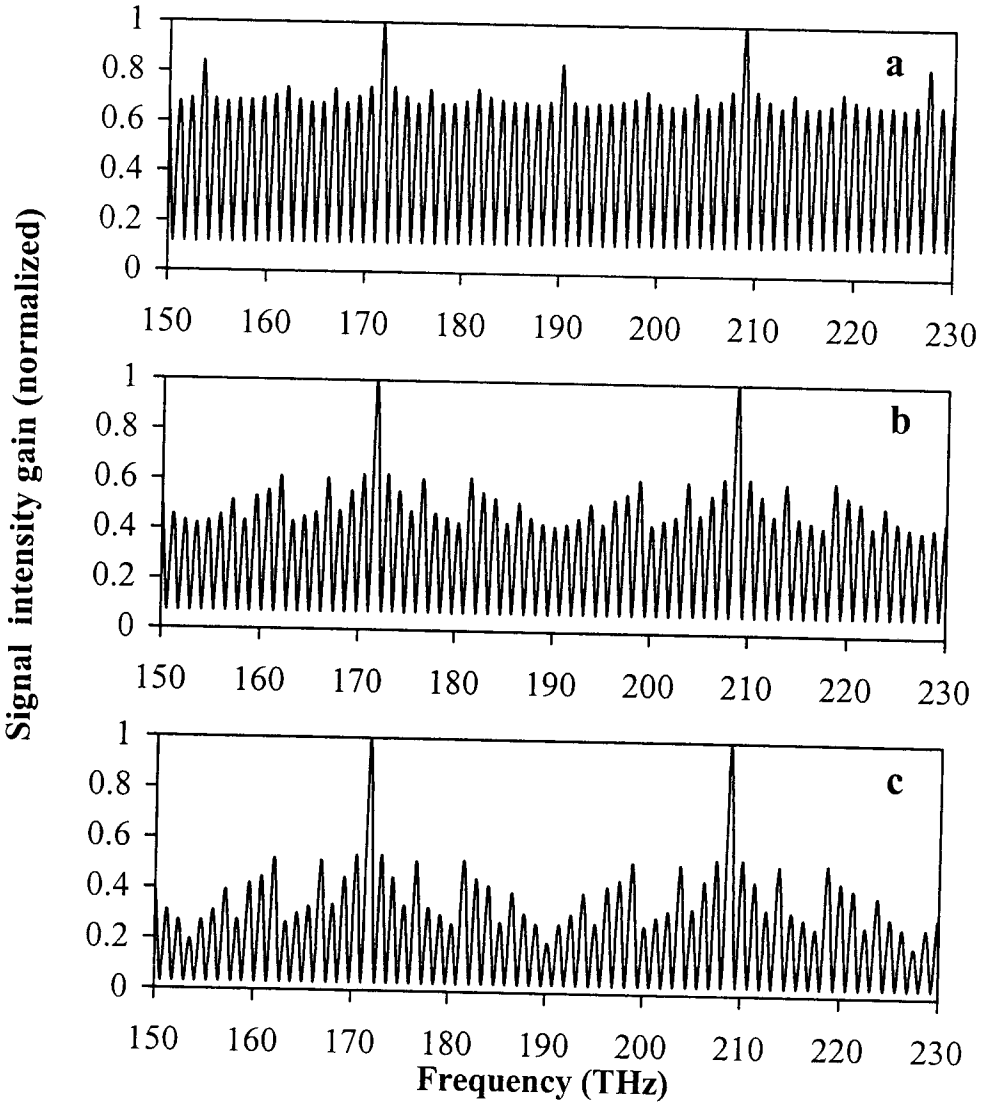

Fig. 2. Signal intensity gain (normalized) as a function of frequency for different G values ($\varphi =$ 40°) **a** $G = 1$, **b** $G = 5$, **c** $G = 40$.

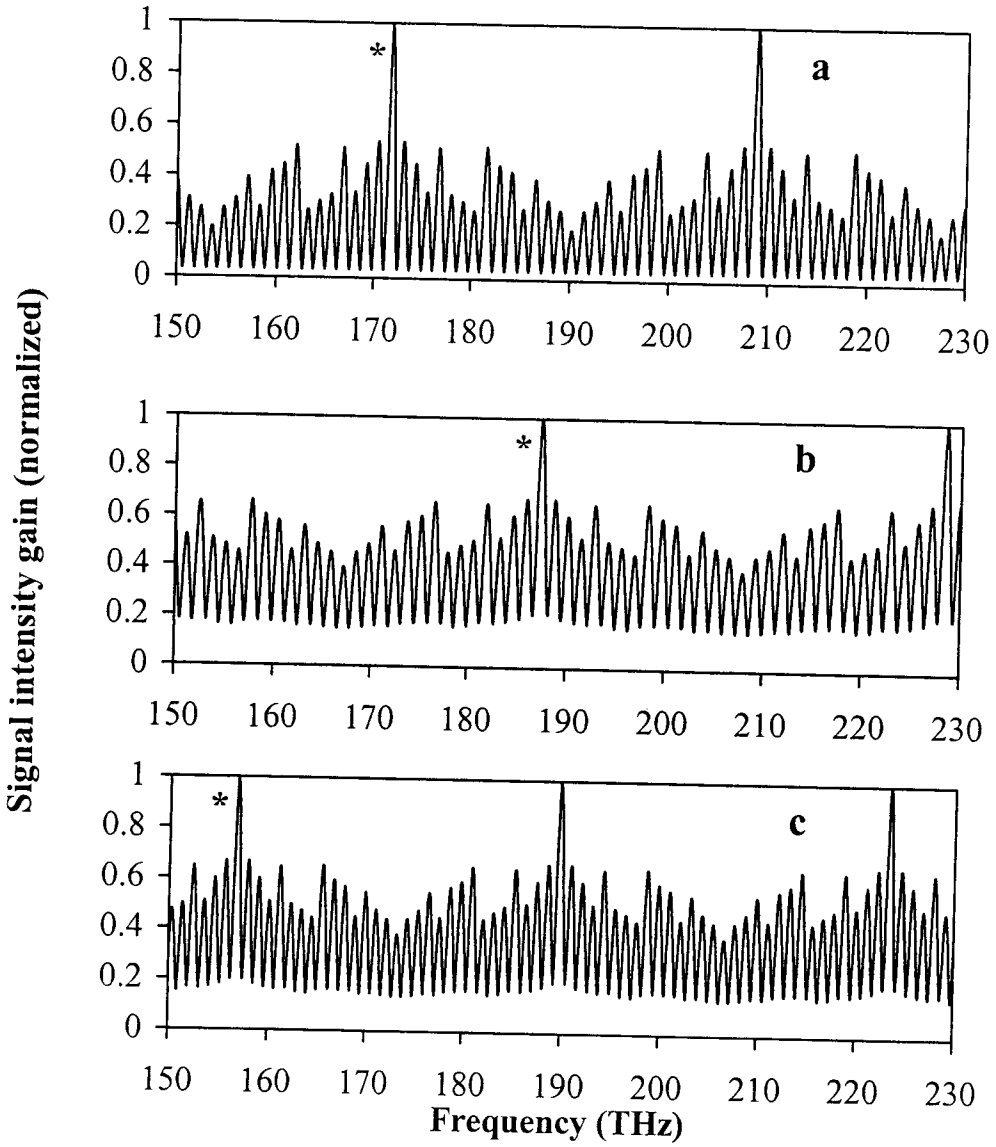

Fig. 3. Signal intensity gain (normalized) as a function of frequency (* transmission maximum tuning): **a** $\varphi = 40°$, **b** $\varphi = 23°$, **c** $\varphi = 58°$.

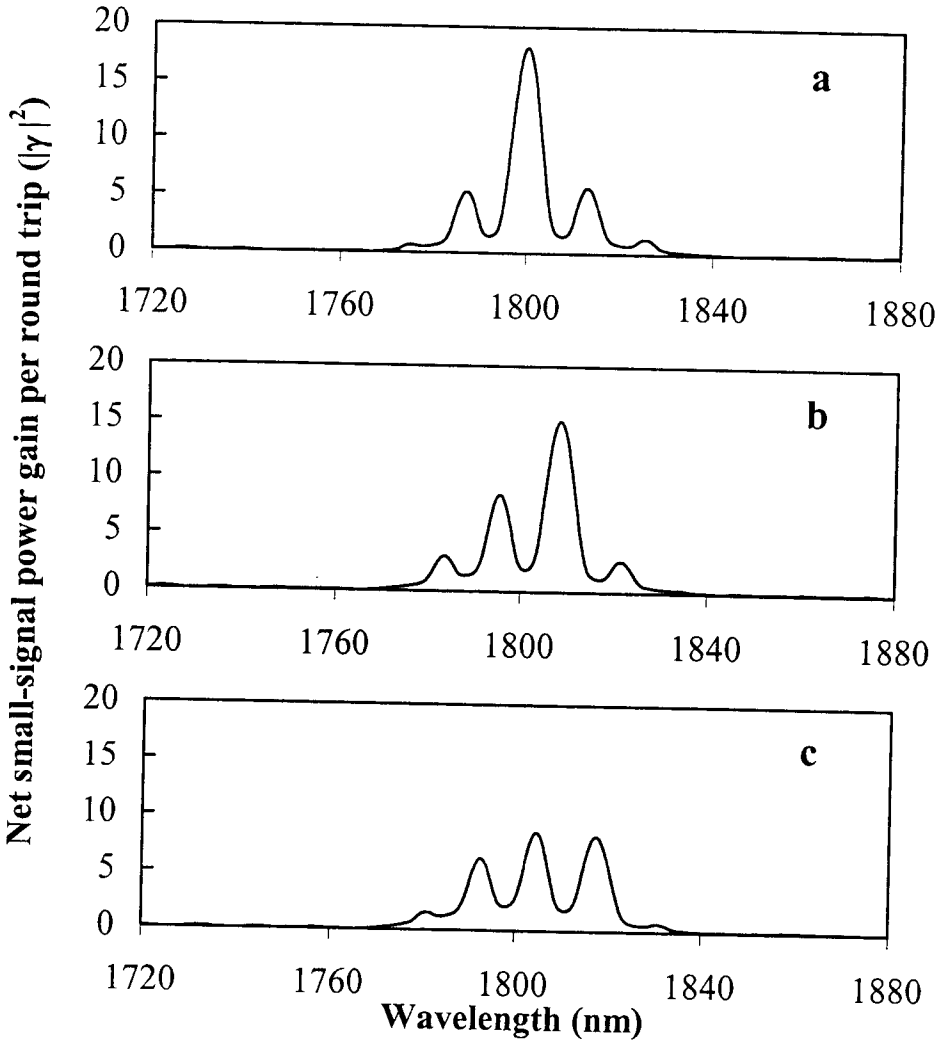

Fig. 4. Net small-signal power gain per round-trip, ($|\gamma|^2$), as a function of wavelength (including output coupling reflection coefficients: $r_S = r_P = \sqrt{0.5}$): **a** $\varphi = 45.6°$, **b** $\varphi = 46.5°$, **c** $\varphi = 47.5°$.

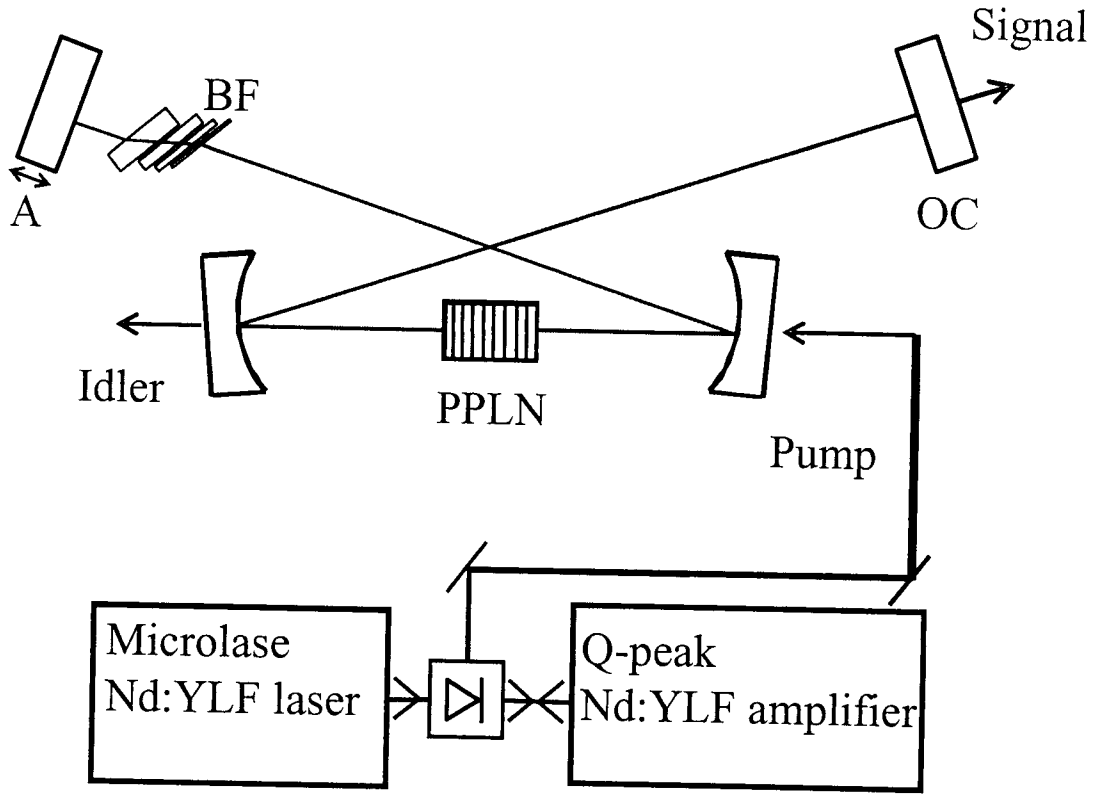

Fig. 5. Schematic of the optical parametric oscillator: OC- output coupler; BF- 4-plate birefringent filter; PPLN- periodically poled lithium niobate crystal; A- back mirror used to resynchronize cavity length.

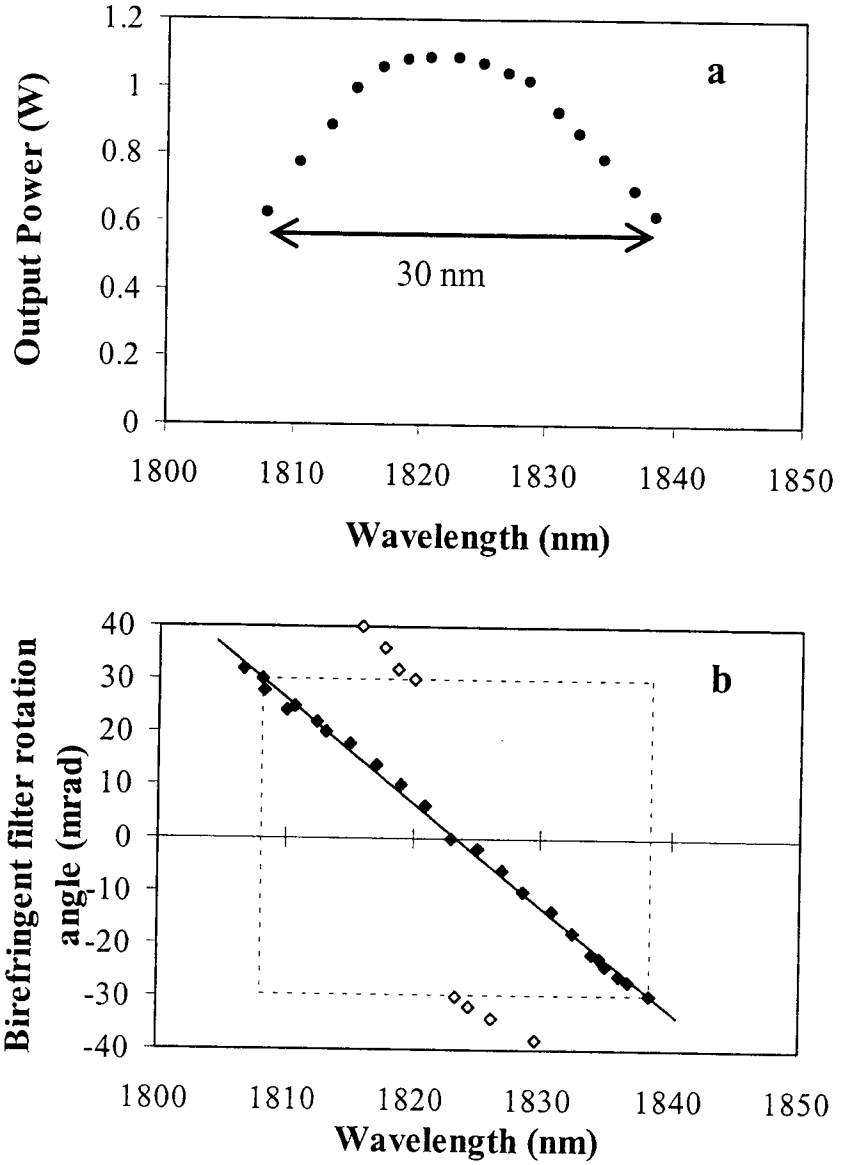

Fig. 6. **a** Signal output power and **b** Birefringent filter rotation angle as a function of wavelength; central tuning peak (filled diamonds), subsidiary maximum tuning peak (unfilled diamonds).

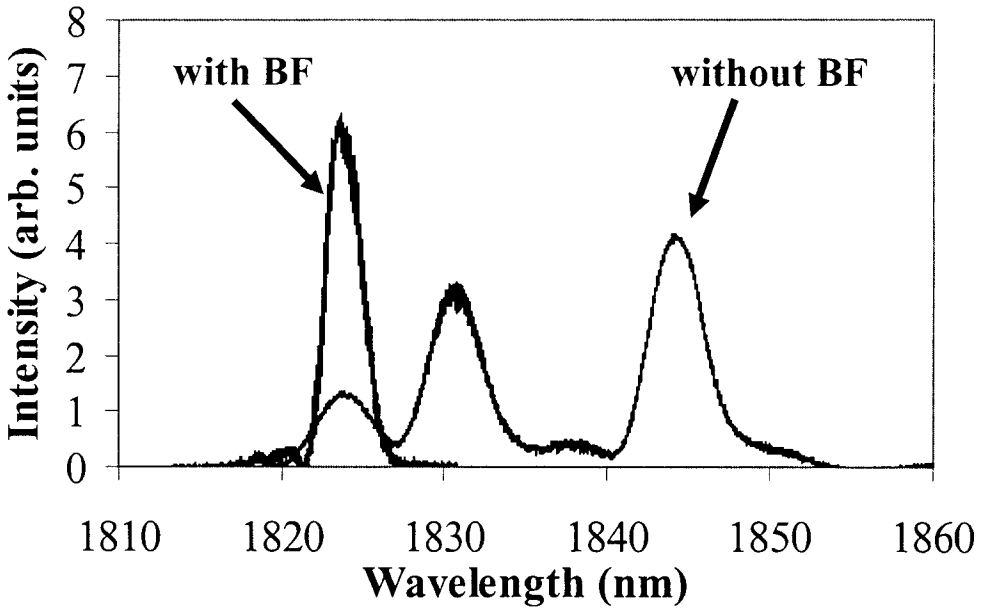

Fig. 7. Typical signal output spectrum with and without the intracavity birefringent filter.